Author's personal copy

Chapter 6

# Chemical Thermodynamics and the Study of Magmas

Mark S. Ghiorso
*OFM Research, Seattle, WA, USA*

Guilherme A.R. Gualda
*Earth and Environmental Sciences, Vanderbilt University, Nashville, TN, USA*

## Chapter Outline



## GLOSSARY

**activity** A thermodynamic measure of the energetically effective concentration of a component in a solution.

**chemical potential** A thermodynamic quantity that describes how the Gibbs free energy of the system changes by addition of one mole of a system component; formally the partial derivative of the Gibbs free energy with respect to the number of moles of a particular component, evaluated at constant temperature, pressure, and the molar abundances of all other components in the system.

**(thermodynamic) component** An independent variable that describes the abundance of a chemical constituent in a thermodynamic system.

**enthalpy** A thermodynamic potential that characterizes the equilibrium state under conditions of fixed entropy content, pressure, and bulk composition; the "heat content" of a thermodynamic system at fixed pressure; this thermodynamic potential is minimized when entropy, pressure and bulk composition are set, with other thermodynamic quantities (e.g., temperature, volume, etc.) being derived quantities.

**entropy** In an equilibrium (reversible) state, a measure of the total heat content of a thermodynamic system; under more general (irreversible) conditions, a measure related to the energetic drive (the chemical affinity) that brings a system to an equilibrium state.

**equilibrium state** The state under which a thermodynamic system can no longer evolve; a state of rest characterized by a global minimum in the thermodynamic potentials (e.g., Gibbs free energy, enthalpy, Helmholtz free energy) of the system.

**fugacity** The energetically effective partial pressure of a component in a thermodynamic system.

**Gibbs free energy** A thermodynamic potential that characterizes the equilibrium state under conditions of fixed temperature, pressure, and bulk composition; this thermodynamic potential is minimized when temperature, pressure and bulk composition are set, with other thermodynamic quantities (e.g., entropy, volume, etc.) being derived quantities.

**Gibbs–Duhem relation** A differential equation that relates variation in the chemical potentials of system components to changes in temperature or pressure; a more generalized statement of the petrologic phase rule.

**Helmholtz free energy** A thermodynamic potential that characterizes equilibrium under conditions of fixed temperature, volume, and bulk composition; this thermodynamic potential is minimized when temperature, volume and bulk composition are set, with other thermodynamic quantities (e.g., entropy, pressure, etc.) being derived quantities.

**The Encyclopedia of Volcanoes.** http://dx.doi.org/10.1016/B978-0-12-385938-9.00006-7
Copyright © 2015 Elsevier Inc. All rights reserved.



The Encyclopedia of Volcanoes, Second Edition, 2015, 143–161

Author's personal copy



**internal energy** A thermodynamic potential that characterizes equilibrium under conditions of fixed entropy content, volume, and bulk composition; this thermodynamic potential is minimized when entropy, volume and bulk composition are set, with other thermodynamic quantities (e.g., temperature, pressure, etc.) being derived quantities.

**isenthalpic process** A process in a thermodynamic system at fixed enthalpy content; a reversible adiabatic process at fixed pressure.

**isentropic process** A process in a thermodynamic system at fixed entropy content; any reversible adiabatic process.

**isochoric process** A process in a thermodynamic system at fixed volume.

**Korzhinskii potential** Any thermodynamic potential applicable to a system that is open to mass transfer of a perfectly mobile component across its boundaries; the potential is defined in such a way that the energetic properties of that mobile component are fixed externally and imposed upon the thermodynamic system.

**latent heat** Heat generated by a system as a result of a change in the thermodynamic state of a phase (e.g., crystallization of a magma).

**(thermodynamic) phase** Any compositionally homogeneous macroscopic region of a thermodynamic system.

**(thermodynamic) potential** An energetic measure of a thermodynamic system whose value is uniquely determined by a set of independent variables (i.e., the state of the system); a function that depends only on the current state of the system, and not on the manner in which the system acquired that state.

**sensible heat** Heat generated by a system as a result of changing the temperature in the absence of a change in the thermodynamic state of a phase (see latent heat).

**(thermodynamic) system** A macroscopic region that contains a collection of one or more phases; the system is closed if the boundary is impermeable to mass transfer.

## 1. INTRODUCTION

Chemical thermodynamics provides a theoretical framework that relates the composition of a **system** to its energy. A system is something that you are interested in studying. It can be broadly defined, as for example a magma body residing in the shallow crust, or narrowly focused, as a phenocryst or a rock. Composition in the system need not be homogeneously distributed, nor even contiguous. In chemical thermodynamics, we speak of the system being partitioned into compositionally homogeneous regions and refer to these as **phases**. We express the composition of the system in terms of a linearly independent set of variables, called **components**. The chemical thermodynamics relates how the energy of the system varies as components are partitioned between the phases and as the proportions of phases vary. This relationship is often nonintuitive; gravity is intuitive, Newton's laws are intuitive, but how the structure of a material and its composition determine its **potential** energy is not. The practical challenge of chemical thermodynamics when applied to magmatic systems is to illuminate as clearly and simply as possible how the energy of the system relates to its phase assemblage.

It is important to appreciate that chemical thermodynamics is applicable to a dynamically evolving system. The common perception is that thermodynamics is the study of the **equilibrium state**, that is, the state of the system for which the energy is at a minimum and from which there can be no further spontaneous evolution of phase compositions and proportions. This view stems from the fact that the principles of thermodynamics uniquely characterize the system at equilibrium, which is determined by minimizing some energetic measure of the system. Yet, thermodynamics allows us to assess the energy of a system in all states, not just the equilibrium one; it thus allows calculation of differences in energy between diverse disequilibrium states and the unique equilibrium state of the system. In this way, chemical thermodynamics gives us a measure of the energetic drive to achieve an equilibrium state, which through the application of kinetic theory, can inform the rates of chemical reactions and the timescales of system evolution.

Despite this direct connection to kinetics, in the application of chemical thermodynamics to magmatic systems we are usually concerned with the equilibrium state. The estimation of the temperature and pressure of coexistence between phases (geothermometry and geobarometry), the analysis of trace element partitioning between phases, the modeling of volatile phase saturation in silicate liquids, and the estimation of phase stabilities and elemental partitioning between phases, all assume that the system of interest is at equilibrium. Even computational tools that do not conform to the theory of thermodynamics still assume an underlying state of equilibrium. While tools may or may not be based upon computational thermodynamics, those rooted in the foundations of thermodynamics generate the most comprehensive view of elemental partitioning in the system. There is an intrinsic advantage of using a long-established (and never refuted!) theory for the dependence of composition, temperature, and pressure on energy; thermodynamics provides constraints on the functional form of the underlying mathematical expressions, which in turn reveals the best method of extrapolation of experimental data sets.

In this chapter we cannot make an encompassing review of the application of chemical thermodynamics to magmatic systems, but instead we will focus on an overview of the application of thermodynamics to the estimation of phase relations in magmatic systems, utilizing a broad spectrum of boundary constraints. Additionally, we will provide a summary of available tools in computational thermodynamics for the calculation of phase relations, volatile solubilities, and geothermometry and geobarometry. For comprehensive treatments of the chemical thermodynamics, presented with an orientation

Author's personal copy



**TABLE 6.1** Thermodynamic Potentials and Their Differential Forms

| Name | Independent Variables | Definition | Differential | |
|---|---|---|---|---|
| Gibbs free energy ($G$) | $T$, $P$, $n_1$, $n_2$,…, $n_c$ | $G = E - TS + PV$ | $dG = -SdT + VdP + \sum_i^c \mu_i dn_i$ | Isobaric crystallization |
| Korzhinskii oxygen ($L$) | $T$, $P$, $n_1$, $n_2$,…, $n_c$ for all components except $O_2$, $\mu_{O_2}$ | $L = G - n_{O_2}\mu_{O_2}$ | $dG = -SdT + VdP + \sum_{i\neq O_2}^c \mu_i dn_i + n_{O_2} d\mu_{O_2}$ | Isobaric, fixed $f_{O_2}$ crystallization |
| Enthalpy ($H$) | $S$, $P$, $n_1$, $n_2$,…, $n_c$ | $H = G + TS$ | $dH = TdS + VdP + \sum_i^c \mu_i dn_i$ | Magma mixing, wall rock assimilation |
| Helmholtz free energy ($A$) | $T$, $V$, $n_1$, $n_2$,…, $n_c$ | $A = G - PV$ | $dA = -SdT - PdV + \sum_i^c \mu_i dn_i$ | Isochoric (constant volume) crystallization |
| Internal energy ($E$) | $S$, $V$, $n_1$, $n_2$,…, $n_c$ | $E = G + TS - PV$ | $DE = TdS - PdV + \sum_i^c \mu_i dn_i$ | Crystallization by heat loss under variable volume constraints |

In the above table $S$ denotes the entropy of the system.

directed to the earth sciences, the reader should consult the excellent texts by Ganguly (2008) and Spear (1993). The classic texts by Pitzer and Brewer (1961) and Prigogine and Defay (1954) are timeless and definitive reference works.

## 2. THERMODYNAMIC POTENTIALS AND MODELING THE EQUILIBRIUM STATE

Solution of most problems in chemical thermodynamics rests on the exercise of calculating an equilibrium assemblage and its properties. This is done through the minimization of a thermodynamic potential (or state function), a measure of the energy content of the system as a function of a set of independent variables (see Table 6.1). The practical question is then which thermodynamic potential is appropriate in which scenario.

The Gibbs[1] free energy ($G$) is the thermodynamic potential that is minimal in a chemical system at equilibrium for the *necessary* conditions of fixed bulk composition, temperature ($T$), and pressure ($P$). The omnipresence of the **Gibbs free energy** in discussions of chemical thermodynamics in earth sciences suggests some higher standing for this potential. This is not so. The apparent obsession for the Gibbs free energy is simply due to (1) the fact that it is relatively easy to perform experiments at fixed $T$ and $P$ in the laboratory and (2) the fact that it is in many cases reasonable to assume that geologic processes take place at fixed $T$ and $P$.

The necessary conditions associated with any thermodynamic potential are essential, and should be understood and applied with care. An open system, e.g., one for which oxygen or hydrogen transfer occurs across the boundaries, or for which a phase or part of a phase is sequestered from chemical communication with the other phases in the system, does not have fixed bulk composition. Such a system can still be in equilibrium, but the necessary conditions must be altered to account for mass transfer across the permeable boundary. In this case, the Gibbs free energy is not the thermodynamic potential of choice. Thermodynamic potentials that are applicable to equilibrium calculations in open systems are called **Korzhinskii potentials**[2] (Ghiorso and Kelemen, 1987) and may be constructed via suitable mathematical transformations of the Gibbs free energy. The reader is referred to the discussion in Ganguly (2008, p. 53) or Callen (1985, Chapter 5) on the method of Legendre transforms for more details. An open system is at equilibrium when the **chemical potential** (μ, definition below) of the mobile component is specified and fixed. A typical example that is applicable to magmatic systems involves equilibrium calculations at fixed redox state. The redox state of a

1 Josiah Willard Gibbs, 1839–1903, see the preface of Bumstead and Van Name (1906).

2 After Dmitri Sergeyevich Korzhinskii, 1899–1985, a petrologist who first formulated and applied the phase rule to rock systems open to volatile transfer.

Author's personal copy



magma is generally specified by constraining the oxygen **fugacity** ($f_{O_2}$), which is simply the "effective" partial pressure of oxygen ($p_{O_2}$); the difference between $f_{O_2}$ and $p_{O_2}$ is due to energetic interaction between oxygen and other system components. The fugacity can be greater than or less than the partial pressure, depending on whether the system energy is raised or lowered by the energetic interaction; the specific relation requires experimental measurement or first-principles computational assessment. The oxygen fugacity is related to the chemical potential of oxygen via the definition

$$\mu_{O_2} = \mu^0_{O_2} + RT \ln \frac{f_{O_2}}{f^0_{O_2}} \tag{6.1}$$

where $R$ is the universal gas constant and the superscript zero denotes the *standard state*, which generally refers to the properties of the pure substance[3]. Formally, the chemical potential is defined as the partial derivative of the Gibbs free energy with respect to the molar concentration of a component in the system:

$$\mu_{O_2} = \left(\frac{\partial G}{\partial n_{O_2}}\right)_{T,P,n_{i\neq O_2}} \tag{6.2}$$

The derivative is taken while holding $T$, $P$, and the concentrations of all other components in the system constant. Physically, the chemical potential assesses the infinitesimal change in the Gibbs free energy of the system associated with an infinitesimal increase in the concentration of the specified component. The chemical potential is the essence of chemical thermodynamics. All we desire to know about the relation between composition and energy is embodied in the system chemical potentials. Their definition is simple, and the great triumph of Gibbs. Their practical calculation is complex and often elusive, but nevertheless represents the holy grail of chemical thermodynamic modeling and the focus of attention of practitioners of chemical thermodynamics for over a century.

Gibbs (1878; eq. 88, p. 87 in Bumstead and van Name, 1906) derived a remarkable equation (which we now know as the **Gibbs–Duhem relation**) that establishes that in a system at equilibrium, the chemical potential of a given component must be the same in all phases. This condition is often taken as the definition of an equilibrium state, and is equivalent to the previously stated criterion that the Gibbs free energy of the system is minimal at equilibrium.

As stated above, equilibrium in an open system can be calculated by constructing a Korzhinskii potential for the case where the chemical potential of the mobile component is specified. In our example case of a fixed oxygen redox state, this potential ($L$, see Table 6.1 and Ghiorso and Kelemen, 1987) is minimal at equilibrium when $T$, $P$, $\mu_{O_2}$, and the concentrations of all other system components are held fixed. Oxygen is released or absorbed across the system boundary in order to maintain the fixed chemical potential constraint. It is worth recalling that a large number of experimental determinations of phase equilibria in magmatic systems are performed at fixed oxygen redox

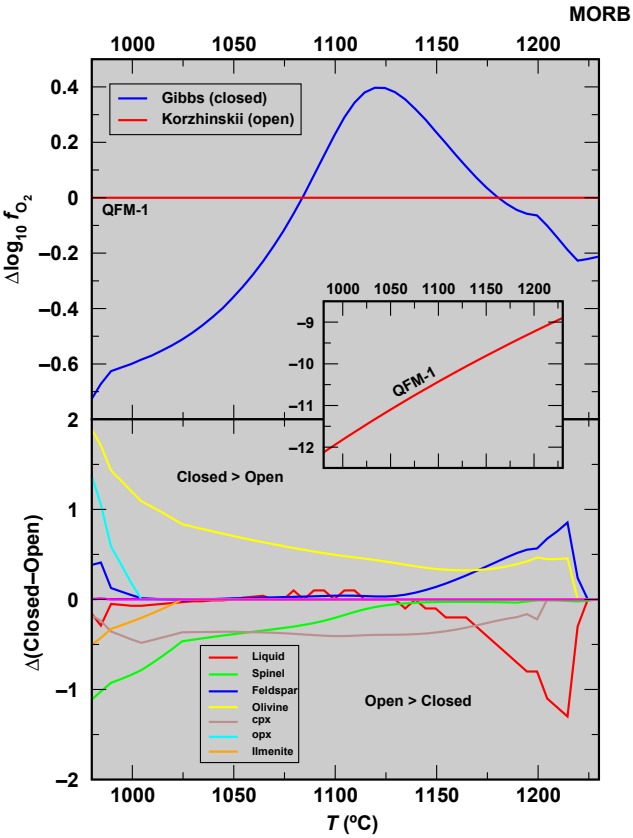


**FIGURE 6.1** Equilibrium crystallization of MORB under closed-system conditions (minimization of the Gibbs free energy) and open-system conditions (boundary open to oxygen transfer; minimization of the Korzhinskii potential). Top panel: redox state of the system, expressed as the base 10 logarithm ($\log_{10}$) of the fugacity of $O_2$ ($f_{O_2}$) relative to the quartz–fayalite–magnetite buffer minus one $\log_{10}$ unit (QFM-1), plotted as a function of $T$. Red line shows the open system, blue curve the closed system. Note that the phase assemblage for the closed system is plotted as a function of $T$ in Figure 6.2. The inset shows the variation of absolute $\log_{10} f_{O_2}$ as a function of $T$ for the open system; the oxygen buffer itself is a strong function of temperature over the entire crystallization interval. Lower panel: difference in phase abundances between closed- and open-system evolutions plotted as a function of $T$. Calculations performed using MELTS (Ghiorso and Sack, 1995) with a 5 °C resolution. In the open-system scenario the redox state is buffered. In the closed-system evolution the system initially oxidizes because precipitating solid phases are enriched in ferrous iron relative to ferric iron, thereby lowering the ferrous to total iron ratio of the liquid with crystallization. The oxidation trend is reversed when a solid phase (here magnetite) appears on the liquidus that has a ferrous to total iron ratio lower than that of the liquid. cpx: clinopyroxene, opx: orthopyroxene. *(See Ghiorso and Carmichael (1985) and Ghiorso (1997) for further discussion.)*

3 In this case the chemical potential or the fugacity of pure oxygen gas at the temperature of interest and the specific pressure of 0.1 MPa.

Author's personal copy



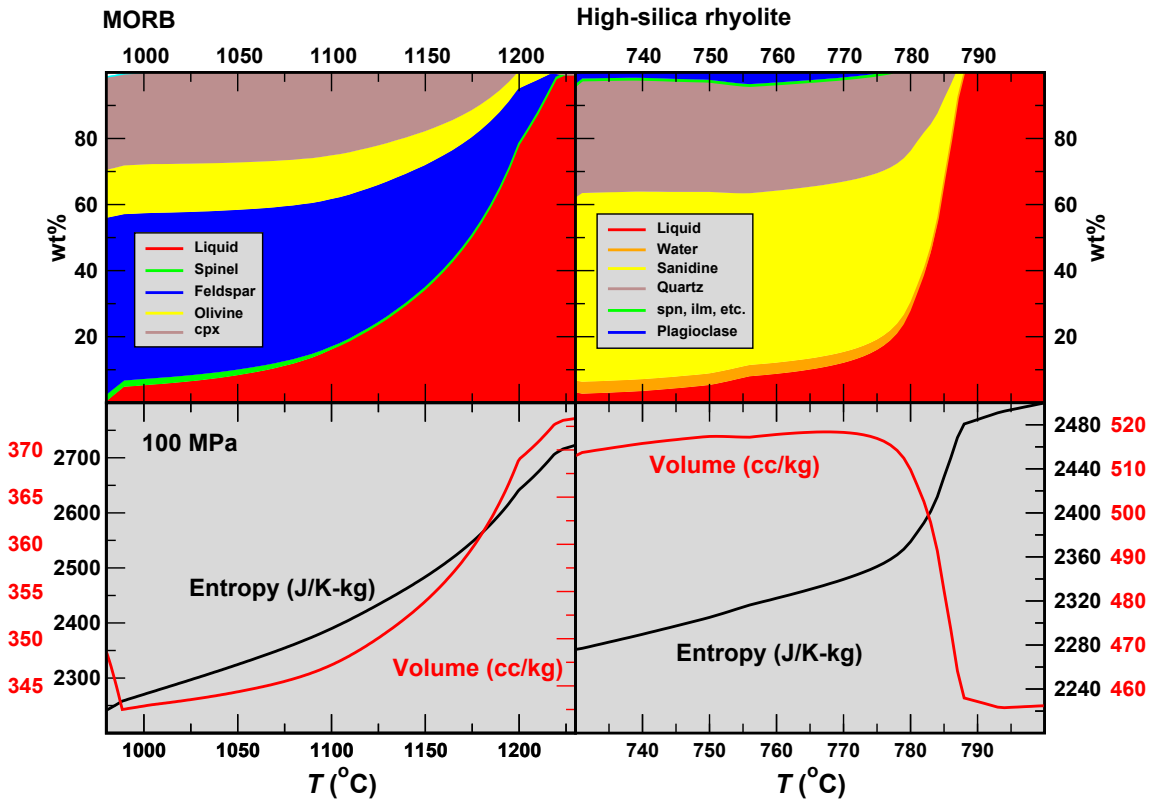


**FIGURE 6.2** Closed system equilibrium crystallization of MORB (left) and high-silica rhyolite (right) as a function of *T* at fixed pressure (100 MPa). Upper panels show phase proportions in wt%. Note that crystallization for the MORB extends over 250 °C, while that for the rhyolite is substantially completed over a 20 °C interval, highlighting the fact that rhyolite bulk composition is near-eutectic in nature. The lower panels show variation in entropy and volume with *T*. The contribution of latent heat to the entropy production is clearly seen for the rhyolite around the "eutectic," which is not apparent for the MORB composition. The decrease in system volume with crystallization for the MORB case is typical, and contrasts with the rapid increase in volume accompanying volatile exsolution demonstrated by the rhyolite composition. Compare the volume and entropy trends for the high-silica rhyolite with the contour diagrams plotted in Figure 6.4. Calculations are performed using rhyolite-MELTS (Gualda et al., 2012) with a 1 °C resolution. MORB composition (grams): $SiO_2$, 48.68; $TiO_2$, 1.01; $Al_2O_3$, 17.64; $Fe_2O_3$, 0.89; $Cr_2O_3$, 0.042; FeO, 7.59; MgO, 9.1; CaO, 12.45; $Na_2O$, 2.65; $K_2O$, 0.03; $P_2O_5$, 0.08; $H_2O$, 0.2. High-silica rhyolite composition (grams): $SiO_2$, 77.8; $TiO_2$, 0.09; $Al_2O_3$, 12.0; $Fe_2O_3$, 0.196; FeO, 0.474; MgO, 0.04; CaO, 0.45; $Na_2O$, 3.7; $K_2O$, 5.36; $H_2O$, 3.74. cpx: clinopyroxene, ilm: ilmenite, spn: spinel.

state, e.g., with an imposed oxygen fugacity buffer. As such, these experiments seek to minimize the Korzhinskii potential in their quest to describe the equilibrium state.

To illustrate the consequences of Gibbs or Korzhinskii potential minimization on magmatic phase relations, closed- and open-system equilibrium crystallization of Mid-ocean ridge basalt (MORB) magma is illustrated in Figures 6.1 and 6.2. The results are obtained by application of the MELTS (Ghiorso and Sack, 1995; Gualda et al., 2012) thermodynamic modeling software (see below) and illustrate the very different evolution paths experienced by the magma cooling under these alternate constraints. Note that in the closed system scenario the redox state, relative to a fixed oxygen buffer, varies in response to the solid phase assemblage that is crystallizing, with the redox state effectively set by the ratio of ferric to total iron in the liquid phase (Kress and Carmichael, 1991); this ratio varies as a consequence of the differential partitioning of ferrous and ferric iron in the coexisting crystals whose identity and compositions vary as a function of crystallization. Some details are presented in the figure legend. For a more thorough discussion of the redox evolution accompanying magmatic crystallization see Osborn (1959, 1962), Ghiorso and Carmichael (1985), Carmichael and Ghiorso (1990), and Ghiorso (1997).

Not all near-equilibrium magmatic processes and evolution scenarios can best be described as Gibbs or Korzhinskii potential minimization problems, despite the fact that intuitively, we are comfortable with using *T* and *P* as constraint variables in thinking about the state and evolution of magma bodies. This intuition comes naturally from the realization that both variables are common controls on experimental phase relations, both are accessible to our everyday experience, and both are independent of the mass of the system being considered. Our intuition to choose these constraint variables, however, does not always lead us

Author's personal copy



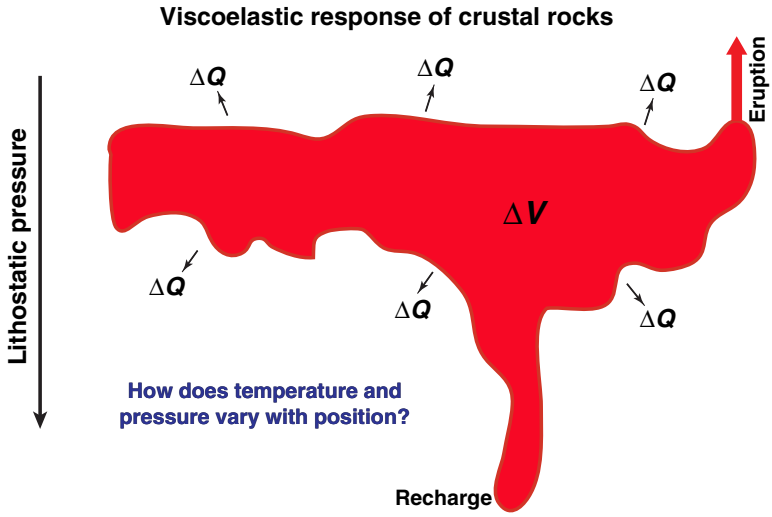


**FIGURE 6.3** Magma body residing in the mid- to shallow-crust. The magma body is surrounded by a viscoelastic container of country rocks. Lithostatic pressure is vertical. Heat is lost ($\Delta Q$) from the magma body to the country rock by cooling. Heat sources within the magma body are derived from sensible and latent contributions. The latter arise from phase change. Cooling also induces volume change ($\Delta V$) of the magma body, similarly arising from sensible and latent contributions. The volume change associated with magmatic crystallization is generally negative, but it can be strongly positive in the case of volatile exsolution at low pressures (see Figure 6.2). If the magma $\Delta V$ accompanying magmatic heat loss is not exactly compensated by the viscoelastic response of the crustal rocks, an internal pressure field will develop within the magma reservoir that does not match the external lithostatic pressure. This pressure differential has the potential of driving either recharge or eruption.

down the best path of understanding how magma bodies respond to the dynamically changing mantle and crustal environments in which they reside. Consider, for example, a magma body in a mid- to shallow-crustal setting. How does this body evolve? Discounting for the moment the consequences of eruption, recharge, and assimilation, the body evolves principally by withdrawal of heat to the country rock (Figure 6.3). The heat withdrawal ($\Delta Q$) takes place by conductive cooling and perhaps some degree of convective removal supported by fluid circulation through the medium of the country rocks. The magma body—regardless of the nature or style of internal convection—partitions this withdrawn heat between lowering the temperature of the body (the portion of heat known as **sensible heat**), crystallizing the liquid phase (the portion known as **latent heat**), and perhaps converting one solid phase to another (generating a negative or positive heat of reaction). The natural operative variable in this scenario is the heat content of the body and *not the temperature*. The temperature is a derived value, determined by the nature of the phase diagram that describes crystallization behavior of the bulk composition of interest. To see how the nature of the phase diagram controls the thermal evolution, compare the evolution of a MORB with that of a high-silica rhyolite, in which crystallization takes place over a very narrow temperature interval, leading to a very nonuniform partitioning between sensible and latent heat (Figure 6.2). Additionally, temperature is critically controlled by the size of the magma reservoir, because heat content is an *extensive* thermodynamic quantity; it depends on mass and hence, the size of the body. It would be more natural, therefore, to consider modeling the evolution of this crustal magma reservoir by specifying the heat content and the pressure of the body, and determining phase compositions, phase abundances, and $T$ as modeled outcomes.

The equilibrium crystallization scenario described in the previous paragraph can easily be modeled. The second law of thermodynamics tells us that for a *reversible* process—a process modeled as a series of equilibrium steps—the change in heat content of a system is equivalent to a change in **entropy** ($S$),

$$\Delta S = \frac{\Delta Q_{rev}}{T} \tag{6.3}$$

The thermodynamic potential that is minimal in a system at equilibrium subject to fixed bulk composition, fixed pressure, and fixed entropy (i.e., heat content) is the **enthalpy** ($H$, see Table 6.1). Consequently, by minimizing the enthalpy of the magma for specified $S$, $P$, and bulk composition, we can calculate the phase compositions, phase proportions, and the temperature of the magma body; the entropy content can be linked to the heat flow out of the body dictated by heat transfer rates through the surrounding country rocks. An example of a calculation of this nature is shown in Figures 6.4 and 6.5. For this calculation the software PhasePlot (www.phaseplot.org) has been utilized, which implements the underlying thermodynamic models of the rhyolite-MELTS package described in Gualda et al. (2012). The bulk composition chosen for this example is a high-silica rhyolite (same

Author's personal copy



composition as in Figure 6.2). For reference, Figure 6.4 shows the equilibrium phase assemblage over a $T-P$ grid, determined by minimizing the Gibbs free energy at each grid point. Phase relations are displayed (see legend), and the entropy of the magma is contoured (inset, upper right); in this case, entropy is a derived quantity. Compare this reference case with the enthalpy minimization case, displayed in Figure 6.5, which shows the equilibrium assemblages on an $S-P$ grid. Again, phase relations are displayed, but in this case the temperature of the magma is a derived quantity and is shown contoured. The observation that derives immediately from examination of these figures is that the release of latent heat of crystallization is evident at the quartz + plagioclase + sanidine + fluid saturated "minimum" (compare with Figure 6.2, which is for a given pressure of 100 MPa—a horizontal section through Figures 6.4 and 6.5). In Figure 6.4, this latent heat effect is shown by the density of entropy contours over a narrow temperature span of 770−730 °C, and in Figure 6.5, by the rotation of temperature contours from the near vertical to horizontal across the entropy span of 2250−2450 J/K-kg. The latent heat is not uniformly distributed across the crystallization interval of this magma type and this has a profound effect on the cooling history. Indeed, if the flux of heat withdrawal was approximately constant across the boundaries of the magma chamber, then entropy would tend to decrease as a linear function of time, and more time would be spent in the relatively uniform temperature regime about the "minimum" than any other interval of crystallization. In other words, in our attempt to understand the time-dependent evolution of magma bodies, entropy is a much better proxy for time than temperature, given that the surrounding rocks control the flux of heat, not the change in temperature. For this bulk composition, the view from an entropy (heat content)-centric perspective is quite different than that derived from a traditional temperature−pressure phase diagram. Nature views magma bodies as reservoirs of dissipating entropy, with temperature going along for the ride.

The inset contour diagram at the lower right in Figure 6.4 shows the variation of magma volume as a function of temperature and pressure. Notice that the magma volume is a strongly nonuniform function of $T$ and $P$, and the reasons for this stem from the fact that the specific volume of phases formed during solidification of the magma are not the same as the specific volumes of the parental liquid phase. Another way of saying this is that the densities of phases produced by crystallization of the magma are not the same as the density of the liquid phase, and the rate of crystallization is not constant. The molar

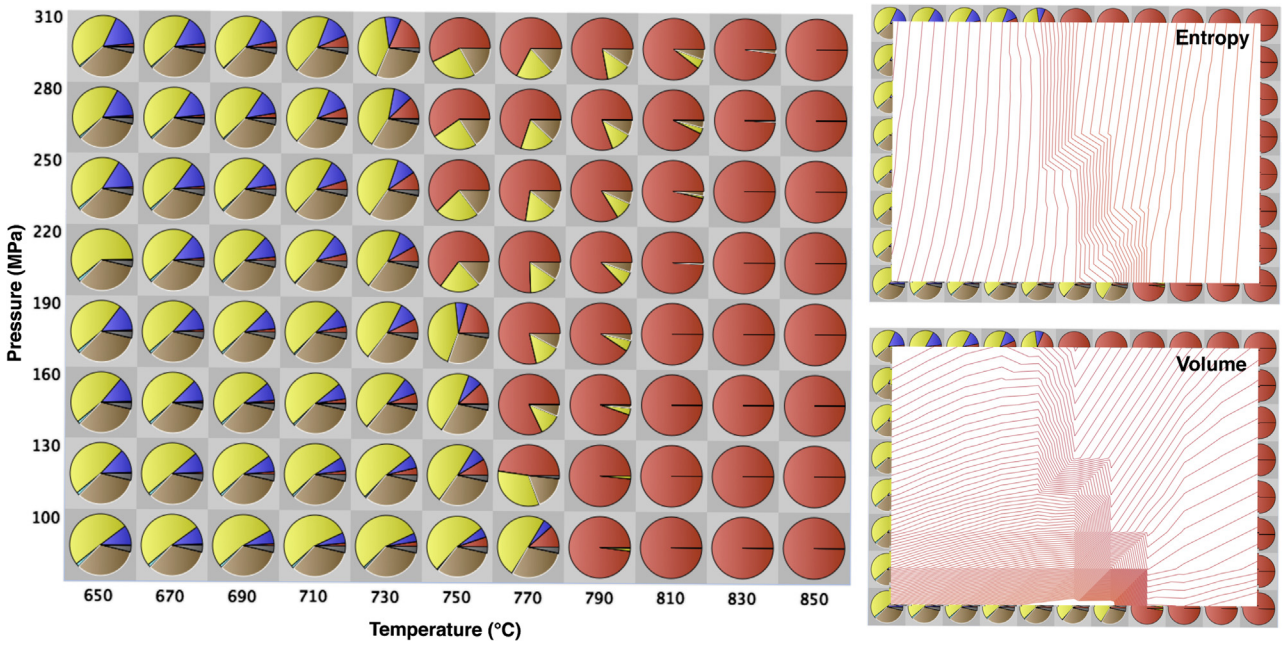


**FIGURE 6.4** Phase relations computed by Gibbs free energy minimization over a temperature−pressure grid of a bulk composition corresponding to a high-silica rhyolite (see legend for Figure 6.2). Phase relations are depicted as pie diagrams centered on each grid node. Colors are: red = melt, yellow = sanidine, brown = quartz, blue = plagioclase, other phases include water, magnetite, pyroxenes, and ilmenite. The phase diagram visualization software PhasePlot (www.phaseplot.org) is used to generate the diagram. The inset on the upper right contours an overlay of the entropy of the system, with 10 J/K-kg contours displayed across the range 2125 J/K-kg (left)−2570 J/K-kg (right). The inset on the lower right contours an overlay of the system volume, with 1 $cm^3$/kg contours displayed across the range 420 $cm^3$/kg (left top)−526 $cm^3$/kg (left bottom). Note that the most rapid change in system entropy and volume is associated with the compact interval of solidification across the narrow band of temperature corresponding to the quartz + two-feldspar + fluid-saturated cotectic. The large and positive volume change across the cotectic is driven entirely by volatile exsolution.

Author's personal copy



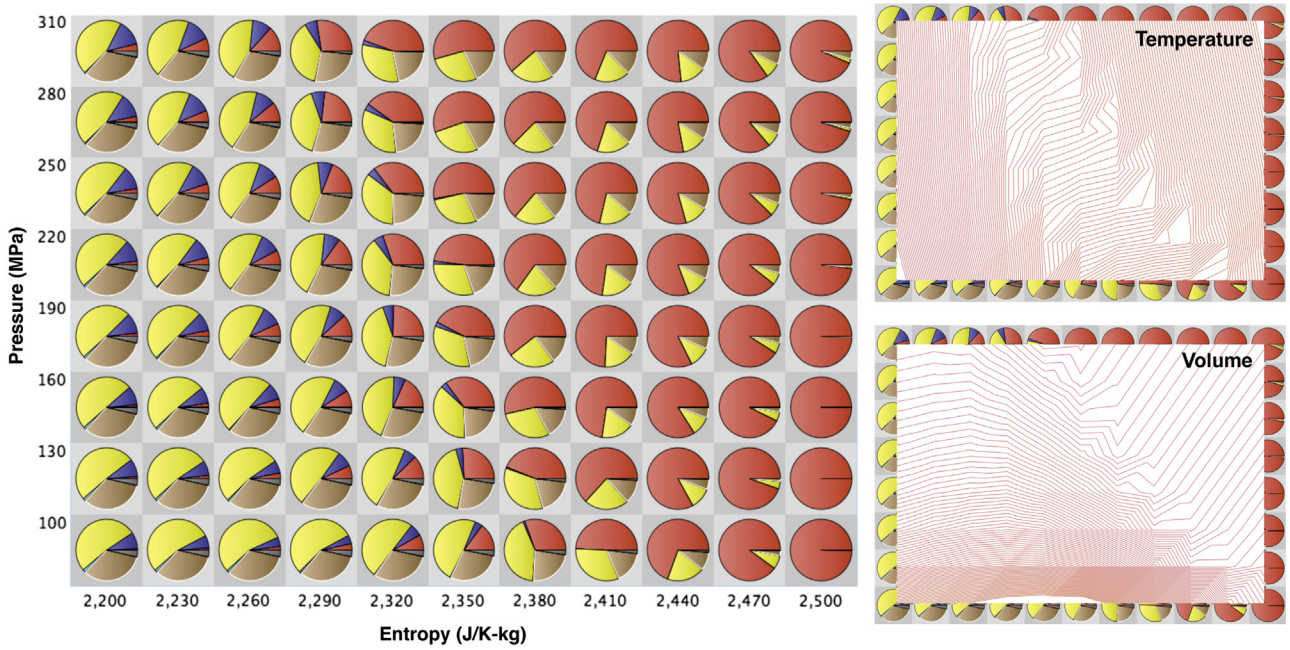


**FIGURE 6.5** Phase relations computed by enthalpy minimization over an entropy−pressure grid of a bulk composition corresponding to a high-silica rhyolite. Phase relations are depicted, labeled, and computed as in Figure 6.4. The inset on the upper right contours an overlay of the temperature of the system, with 1 °C contours displayed across the range 676 °C (left)−818 °C (right). The inset on the lower right contours an overlay of the system volume, with 1 $cm^3$/kg contours displayed across the range 419 $cm^3$/kg (top)−525 $cm^3$/kg (left bottom). Note that the temperature contours change orientation from nearly vertical to nearly horizontal as the quartz + two-feldspar + volatile-saturated cotectic is traversed. Compare the volume contour diagram with that shown in Figure 6.4 and note that the compact volume change in temperature space is extended over a much broader interval of entropy space. As the entropy (or heat content) of the magma is changed, the temperature response is dominated by sensible heat, where the temperature contours are vertical, or latent heat, where the temperature contours approach the horizontal.

volume of a volatile phase (principally $H_2O$−$CO_2$ fluid solutions) is, at shallow crustal pressures, much larger than the partial molar volumes of dissolved $H_2O$ or $CO_2$ in the melt, and the specific volumes of solid phases are generally smaller than the corresponding compositionally equivalent mass of liquid. These generalizations are intriguing because if one views the magma body as residing in a deformable pile of crustal rocks, then the question arises as to whether the crustal container can deform quickly enough to compensate the volume change associated with phase transformations in the solidifying magma and maintain a constant pressure within the magma body. If crustal deformation is not fast enough, a pressure drop or rise in the magma will follow, leading to decoupling of the internal pressure field of the magma body from the lithostatic pressure field of the crustal rocks. The critical thermodynamic variables that govern the internal pressure of the magma are consequently the volume of the magma container, and the bulk compressibility (β; or its inverse the bulk modulus, $K$) of the magmatic liquid + solid + fluid assemblage. The latter quantifies how the volume changes due to a change in applied pressure.

In order to access the consequences of magmatic crystallization on the condition of chamber volume dictated by crustal deformation rates, we must find a thermodynamic potential that is minimal under conditions of specified volume ($V$), temperature, and bulk composition. That potential is the **Helmholtz free energy** ($A$, see Table 6.1). Minimizing $A$ at fixed $V$, $T$, and bulk composition yields the equilibrium compositions and proportions of phases and values for the dependent quantity pressure. An illustration of this calculation, again for the high-silica rhyolite composition used in Figures 6.2, 6.4, and 6.5, can be performed with PhasePlot and is presented in Figure 6.6. One sees from the pressure contour diagram that overlays the $V$−$T$ phase relation grid (inset, lower right), that pressure changes dramatically as a consequence of exsolution of a volatile phase, a not altogether surprising result given the drastic difference in density of the volatile phase compared with that of the solids and liquids. The pressure contours are subhorizontal in the $V$−$T$ subgrid where volume change is dominated by thermal deflation; pressure contours become vertical where the $\Delta V$ of phase change induced by a temperature drop dominates (see figure legend for additional discussion). A detailed application of Helmholtz minimization to phase equilibria and evolution of the Campanian magma body is presented by Fowler et al. (2007) for the specific end-member case of **isochoric** (constant volume; infinitely rigid crust) crystallization.

Author's personal copy



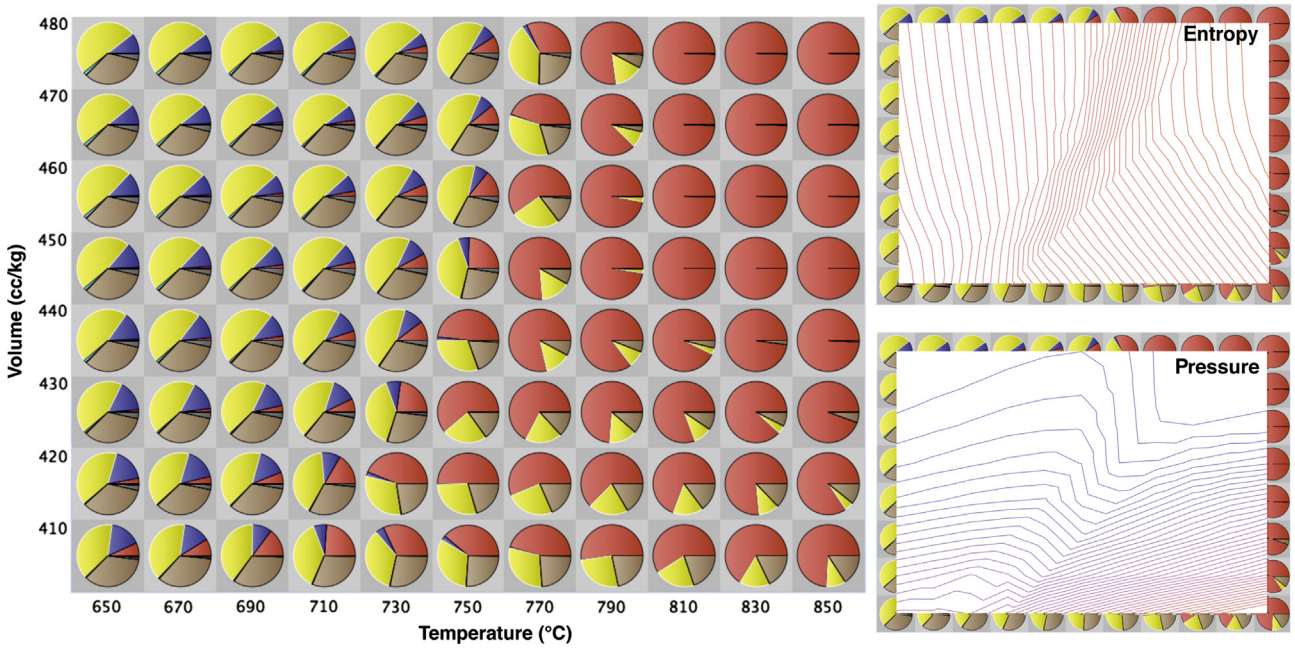


**FIGURE 6.6** Phase relations computed by Helmholtz free minimization over a temperature−volume grid of a bulk composition corresponding to a high-silica rhyolite. Phase relations are depicted, labeled, and computed as in Figure 6.4. The inset on the upper right contours an overlay of the entropy of the system, with 10 J/K-kg contours displayed across the range 2100 J/K-kg (left)−2570 J/K-kg (right). The inset on the lower right contours an overlay of the system pressure, with 20 MPa contours displayed across the range 76 MPa (right top)−966 MPa (right bottom). The abrupt change in the slope of the pressure contours corresponds to the onset of volatile saturation.

None of the results presented in Figures 6.4, 6.5, or 6.6 bear the greatest fidelity to the more realistic boundary constraints on upper crustal magma chamber evolution that are dictated by simultaneous and competing rates of heat withdrawal and crustal deformation. The operative thermodynamic variables in this general case are the total heat content of the magma (the entropy in the equilibrium approximation) and the chamber volume. The thermodynamic potential that is minimal for specified values of entropy, volume, and bulk composition is the **internal energy** ($E$, see Table 6.1). Minimizing $E$ at fixed $S$, $V$, and bulk composition yields the equilibrium proportions and compositions of phases in the system as well as values for the dependent variables, $T$ and $P$. We illustrate such a calculation with results from PhasePlot in Figure 6.7, again using the same high-silica rhyolite composition as before. Note that the temperature−pressure field changes in a nonlinear fashion over the $S-V$ grid. The key thermodynamic quantities that translate heat and volume to temperature and pressure are the isobaric heat capacity ($C_P$) and, as noted above, the isothermal compressibility (β). Both quantities have been measured experimentally (for compilations see Lange and Carmichael, 1990; Ghiorso and Kress, 2004). $S$ and $V$ are the "natural" thermodynamic variables for understanding the thermal and mechanical coupling between the state of a magma body and surrounding environment. They are not the intuitive variables that we are used to thinking and working with. But, viewing the evolution of a magma body as a pool of dissipating entropy residing in a deforming container is the proper mind-set for understanding the thermodynamic constraints under which the system evolves.

How the pressure−temperature field of a magma body evolves in detail will be mandated—at both a local and global scale—by heat content and volume constraints, which are in turn a product of a combination of internal and external factors. Phase transformations, or more generally the phase diagram of the magma, dictate the internal contributions to $S$ and $V$, while the mechanics of deformation and the vagaries of heat flow dictate the external factors. Predictions of specific outcomes are difficult to generalize and must be computed by numerical models that couple thermodynamic and dynamic (and kinetic) contributions. Such models are state of the art in computational petrology and beyond the realm of this brief chapter, but several important features of these coupled models should be appreciated. Even the simplest coupled models of magma-body crustal evolution must admit the compressibility of the magmatic fluid, which is commonly ignored by imposing the Boussinesq approximation in standard dynamical modeling. Volume change on phase transformation must appear in a realistic coupled model as must the dependence of the latent heat production on volume fraction of melt. These are first-order physical phenomena

Author's personal copy



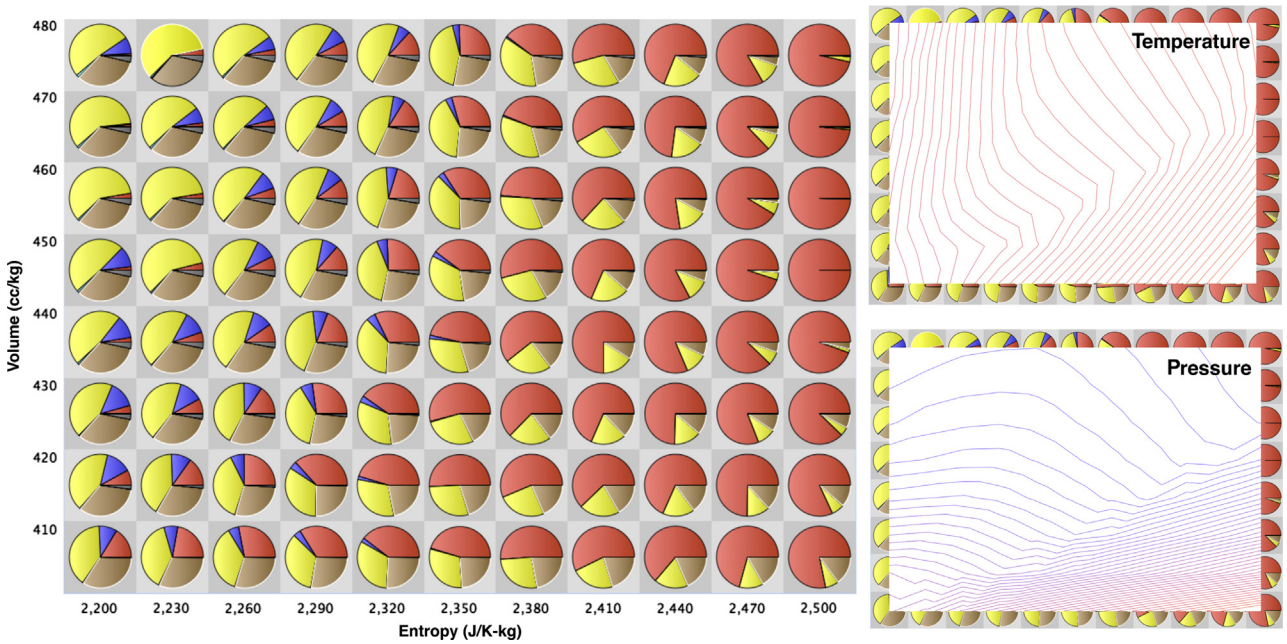


**FIGURE 6.7** Phase relations computed by internal energy minimization over an entropy−volume grid of a bulk composition corresponding to a high-silica rhyolite. Phase relations are depicted, labeled, and computed as in Figure 6.4. The inset on the upper right contours an overlay of the temperature of the system, with 5 °C contours displayed across the range 680 °C (left)−860 °C (right). The inset on the lower right contours an overlay of the system pressure, with 20 MPa contours displayed across the range 76 MPa (top)−992 MPa (right bottom).

that prescribe the evolution of the $T-P$ field in the magma reservoir, and all these phenomena are dictated by the phase diagram of the magma. Phase diagrams can be determined by experiment under controlled $T$ and $P$ conditions. We make thermodynamic models of these data—meaning that we generate expressions for Gibbs free energies of the phases that contribute to the phase diagram. We require the theory of chemical thermodynamics, however, to utilize these data in the broadest possible context, which allows us to calculate outcomes that are not directly obtainable from experiment, but that can be computed in ways that are a direct and internally consistent consequence of the primary observations.

## 3. THE MINIMIZATION OF A THERMODYNAMIC POTENTIAL

Often the statement that the equilibrium state of a system is given by the minimum in an appropriately constrained thermodynamic potential leaves the student in a quandary. How is that minimization actually done? It turns out that the method is not really all that complicated, but in most cases the process is tedious, and inevitably for real systems, must be accomplished by iterative approximation.

Any thermodynamic potential that is minimal in an equilibrium state can be thought of as defining a geometrical or topographical landscape with hills and valleys (Figure 6.8). The height of the landscape is the value of the system energy. The coordinates of the landscape (and in general, there are more than two) constitute the temperature or entropy, pressure or volume, and independent composition variables of the system. In thermodynamic modeling we seek the lowest point on this energy landscape (Figure 6.8). All other points represent states that are not in

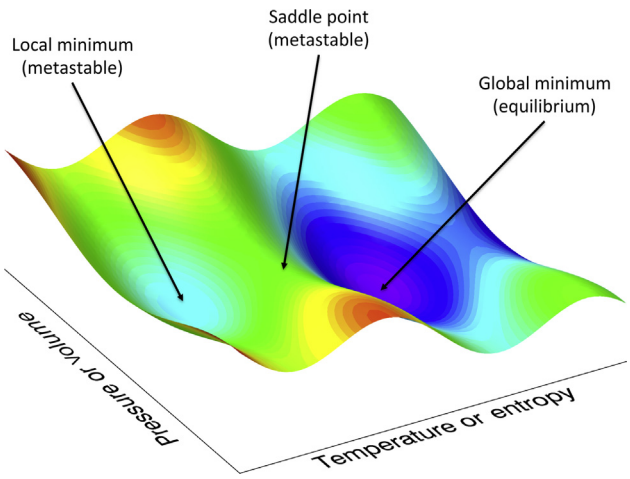


**FIGURE 6.8** Hypothetical thermodynamic potential surface for a one-component system, illustrating an energy landscape with independent variables temperature and pressure ($G$), temperature and volume ($A$), entropy and pressure ($H$), and entropy and volume ($E$). See Table 6.1. Various topological features are displayed. The global minimum is the deepest valley in the energy landscape.

Author's personal copy



equilibrium and correspond to metastable phase assemblages. The system might reside at an apparently stable local minimum and not the global minimum, but under such circumstances it would be metastable (Figure 6.8); the phases may be in exchange equilibrium with respect to one or more components, or some critical phase may be suppressed from the assemblage due to kinetic barriers to its formation.

To determine the equilibrium state of a system the task in computational thermodynamics is twofold: (1) the identity of the equilibrium phase assemblage must be determined and (2) the system components must be partitioned between those phases in order to reduce the energy of the system as much as possible. The first task is the key to success. A global minimum will not be achieved unless the correct phase assemblage is specified. Simply choosing an arbitrary point on an energy landscape and riding downhill to the nearest minimum does not guarantee that you will end up at the global minimum and consequently does not guarantee that the correct equilibrium phase assemblage will be deduced. The procedure that must be employed to assure attainment of an equilibrium assemblage involves a periodic interrogation of the stability or instability of all potential phases that *might contribute* to the assemblage. Identifying the stability condition of a phase *vis-a-vis* a potential assemblage of phases that are candidates for an equilibrium assemblage, can be formulated and solved as an iterative but algebraic problem with a guaranteed solution (Ghiorso, 2013; illustrated also in Figure 6.9). Accordingly, the most complex task of the equilibrium algorithm is the one of finding the minimum energy of the system once a hypothetical phase assemblage has been identified. There are many ways to solve this computational problem. The method employed in PhasePlot or the MELTS family of phase calculators (Ghiorso, 1985; Ghiorso and Sack, 1995) is illustrated in Figure 6.10.

No matter what the order of complexity of the energy landscape for a thermodynamic system, the topology can always be locally approximated about any point of interest by a tangential paraboloid (the multidimensional equivalent of a parabola). This approximation is done by constructing the paraboloid using the first and second derivatives of the true energy surface, evaluating both at the point of interest (see Figure 6.10). The first derivative of the energy surface in practice is a vector and the second derivative is a symmetric matrix of second partial derivatives, but regardless of these details, this quadratic geometrical approximation is always possible. The point of interest, of course, is an initial guess to the phase compositions and proportions as determined utilizing the phase stability algorithms alluded to previously. A minimum of the locally tangential paraboloid can always be located by construction or numerical

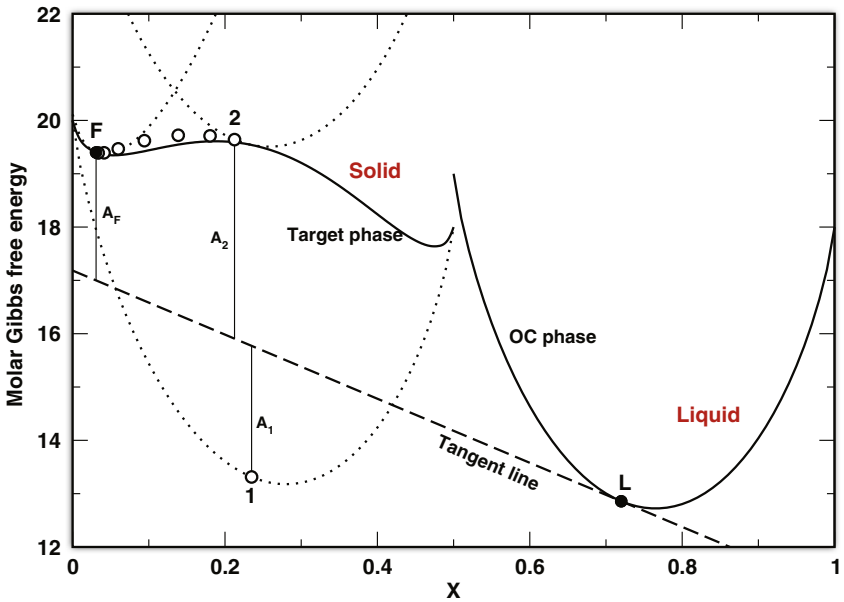


**FIGURE 6.9** Illustration of a saturation state detection algorithm for a solid phase referenced to a liquid phase of composition $X_L$. The Gibbs free energies of the two phases are illustrated by the heavy solid curves. The dashed line labeled "tangent line" is tangent to the liquid phase at "composition" $X_L$. This line has the same slope as the tangent to the target phase at $X_F$. Points 1, 2, etc. refer to the sequence of intermediate solutions that converge to F. The chords labeled $A_i$ are geometrical representations of the chemical affinity, which is a direct measure of the degree to which the solid phase is undersaturated with respect to the liquid phase. When the affinity is zero (i.e., when the tangent line touches both the liquid and solid Gibbs free energy surface) the solid is in equilibrium with the liquid phase. The dotted curves are "ideal mixing" approximations of the solid phase. The algorithm for locating $X_F$ and a value for $A_F$ is taken from Ghiorso (2013). The procedure is to approximate the solid phase as a succession of pseudoideal solutions, until that approximation converges on the properties of the real solution. For implementation details, consult the reference. OC phase: omnicomponent phase.

Author's personal copy



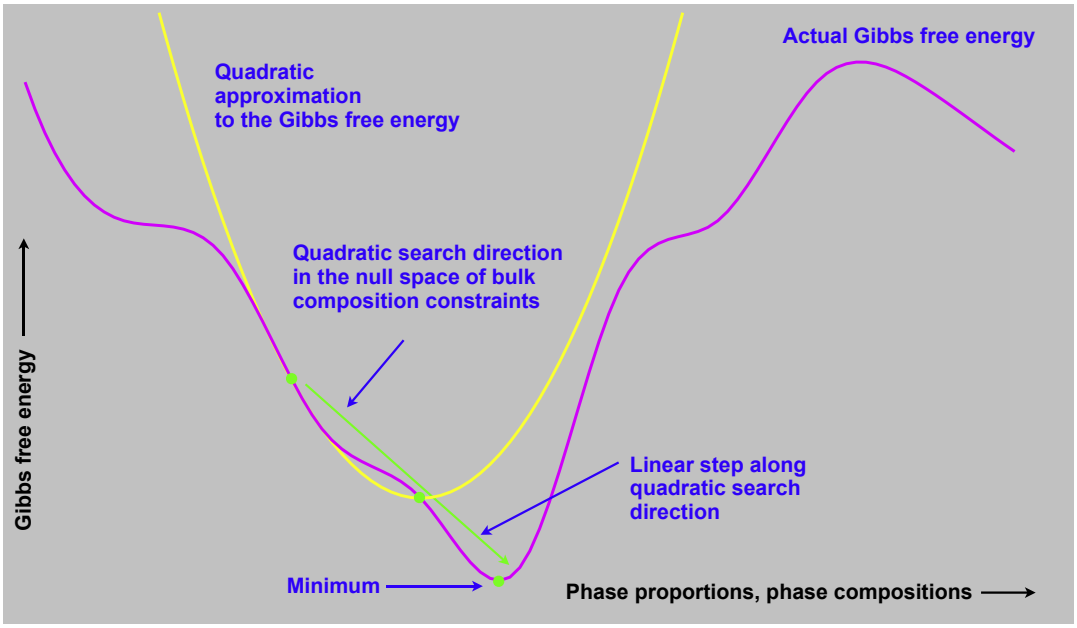


**FIGURE 6.10** The minimum of a thermodynamic potential, like that of the system Gibbs free energy illustrated, is obtained by choosing an initial guess to the energy minimum, illustrated here as the left most filled green circle, and constructing at that point a parabolic approximation to the energy, which has the same first and second derivatives as the energy surface at the point of interest. In this figure that parabolic approximation is shown as a yellow curve. The initial guess must be independently estimated, perhaps using some form of the saturation state algorithm illustrated in Figure 6.9; it consists of approximate phase proportions and compositions that might characterize a good guess of the equilibrium assemblage. A search direction is poised starting from the initial point and projecting through the minimum of the parabolic approximation. A "linear search" is extended along that direction (the illustrated green vector) until a lower point on the actual energy surface is reached; this procedure derives new and better values of phase compositions and proportions. This new "low point" becomes the next guess, and the procedure is repeated until the true minimum is reached. Typically this takes four or five parabolic or "quadratic" iterations. The illustrated algorithm is given in detail in Ghiorso (1985). Mathematically, the method is a concrete example of a projected second-order Newton method.

evaluation. The only complication to this exercise is that the location of the parabolic minimum must satisfy, as did the initial feasible point, all of the imposed constraints that qualify the equilibrium condition. For the Gibbs free energy, these would be fixed $T$, $P$, and bulk composition, and for the Helmholtz energy, fixed $T$, $V$, and bulk composition, etc. The mechanics of imposing these constraints is straightforward and discussed elsewhere (Ghiorso, 1985), but the important thing to understand is that the parabolic minimum is chosen in such a way that the constraints are enforced and the solution is physically viable.

As shown schematically in Figure 6.10, the vector from the initial point of interest to the parabolic minimum is taken as a feasible direction of extrapolation along which a "linear" search is made to locate the lowest position on the energy landscape. Once this location is found, a new paraboloid is constructed tangential to this position and the whole process is repeated until the true minimum is located. Generally, four to five parabolic approximations suffice to locate the true minimum. Once found, phase-stability checks either discredit the minimum by the addition of more stable phases to the assemblage, or verify the minimum as global if no additional phases are found to be more stable than the current assemblage. This procedure can be programed for very rapid execution, particularly if the thermodynamic derivatives of all of the phases involved in the calculation are coded analytically. As an example, execution time for a typical Gibbs free energy minimization in rhyolite-MELTS (Gualda et al., 2012) for a five-phase system with ~25 optimal variables and 10 active constraints requires about 100 ms on a 3-GHz processor.

## 4. COMPUTATIONAL THERMODYNAMICS TOOLS AVAILABLE TO THE VOLCANOLOGIST/IGNEOUS PETROLOGIST

We will end this brief chapter with a summary and notes regarding freely available tools for computational chemical thermodynamics applications in volcanology and igneous petrology. These applications fall into four general categories: (1) geothermometers, geobarometers, and geohygrometers, (2) mineral and melt thermodynamic property calculators, (3) solubility calculators for volatiles in magmatic systems, and (4) phase equilibrium calculators. Our summary is by no means exhaustive, and emphasis has been placed on calculators that are web-based or run on a

Author's personal copy



variety of computer systems. Commercial software products are not included.

## 4.1. Geothermometers, Geobarometers, and Geohygrometers for Magmatic Systems

Geothermometers are tools that utilize compositional partitioning of elements between coexisting phases to infer something quantitative about the temperature under which the assemblage formed. Geobarometers do the same for pressure. Geohygrometers describe the effect of dissolved water in one phase (generally the liquid) on elemental partitioning between the liquid and another coexisting solid phase, allowing estimation of water content in the liquid in equilibrium with the solid. These tools are always calibrated from underlying experimental data sets and generally their formulation is thermodynamically "inspired," but incomplete; the formalism is based on thermodynamic theory but is generally not developed into a complete internally consistent description of the Gibbs free energy of all phases that participate in the assemblage. All geothermometers, geobarometers, and geohygrometers rely on the establishment of exchange equilibrium that governs predictable partitioning of an element or elements of interest between the phases of interest. It is important to bear in mind that two phases can be in exchange equilibrium and still constitute a metastable phase assemblage (e.g., exchange equilibrium could correspond to a local minimum or a saddle point, see Figure 6.8); as noted above, only at the global minimum of the energy landscape is the true equilibrium phase assemblage manifest.

An excellent summary of geothermometers and geobarometers applicable to volcanic rocks is provided in Putirka (2008); see Table 6.2. Also in the table, we list additional sources of information and direct links to other commonly utilized formulations. Of particular note are the Ti-in-quartz (Wark and Watson, 2006) and the Ti-in-zircon (Watson et al., 2006) geothermobarometers. These tools rely on knowing the partitioning behavior of Ti between melt and mineral phases and have wide application in the study of silicic rocks. Both require estimation of the **activity** of $TiO_2$ in the coexisting liquid phase; for this purpose see the method of Ghiorso and Gualda (2012). A number of thermometric calculators derived from solid−solid elemental exchange are also listed in Table 6.2, most notably the elegant method of Andersen et al. (1993; QUILF), which is an example of a generalized geothermobarometric approach that examines elemental partitioning between multiple phases, thereby generating a more reliable estimate of $T$ and $P$ than methods based on a single exchange. The widely utilized Fe−Ti oxide geothermometer and oxygen barometer is also listed. This method relies on the calibration of Fe−Ti

**TABLE 6.2 Computational Thermodynamic Tools**

| Source | Type Notes/URLs |
|---|---|
| Putirka (2008) | Volcanic geothermometers and geobarometers<br>Review and summary. Links to Excel workbook implementations:<br>Clinopyroxene P-T<br>Feldspar-liquid P-T-H2O<br>Mantle Potential Temperatures<br>Olivine and glass thermometers<br>Opx thermobarometers<br>Silica activity barometers<br>Two-feldspar thermometers<br>Two-pyroxene thermobarometers |
| Anderson et al. (2008) | Plutonic geothermometers and geobarometers |
| Wark and Watson (2006), Thomas et al. (2010), Huang and Audetat (2012) | Ti-in-quartz geothermometer and geobarometer<br>TitaniQ |
| Hayden et al. (2008) | Sphene (titanite) geobarometer and geothermometer |
| Watson et al. (2006), Ferry and Watson (2007) | Ti-in-zircon, Zr-in-rutile geothermometer |
| Berman (2007) | Thermobarometric calculations using an extended Berman (1988) database<br>http://serc.carleton.edu/research_education/equilibria/twq.html |
| Tim Holland | Mineral activity models, geothermometers, and geobarometers<br>https://www.esc.cam.ac.uk/research/research-groups/holland<br>(AX: activity models, HBPL: hornblende-plagioclase geothermometer) |
| Ghiorso and Evans (2008) | Fe−Ti oxide geothermometer oxygen barometer<br>http://ctserver.ofm-research.org/OxideGeothrm/OxideGeothrm.php |
| Sack and Ghiorso (1991) | Olivine−spinel geothermometer<br>http://ctserver.ofm-research.org/Olv_Spn_Opx/index.php |
| Lange et al. (2009) | Plagioclase−liquid hygrometer and thermometer<br>http://www.lsa.umich.edu/earth/people/faculty/ci.langerebecca_ci.detail |
| Gualda and Ghiorso (2014) | Quartz + feldspar + melt barometry |
| Andersen et al. (1993) | Multivariate equilibrium assessment QUILF. Program may be downloaded from the journal archives |

(*Continued*)

Author's personal copy



**TABLE 6.2 Computational Thermodynamic Tools—cont'd**

| Source | Type Notes/URLs |
|---|---|
| Berman (1988) | Thermodynamic database: end-member properties, reaction properties, univariant curves http://ctserver.ofm-research.org/ThermoDataSets/Berman.php |
| OFM Research | Sack and Ghiorso mineral solution models http://ctserver.ofm-research.org/phaseProp.html http://melts.ofm-research.org/CalcForms/index.html |
| Kress (1997, 2000, 2007), Kress et al. (2008) | Solution models of sulfide liquids The system O–S–Fe–Ni–Cu |
| OFM Research | Web services: REST and SOAP based http://ctserver.ofm-research.org/webservices.html |
| Newman and Lowenstern (2002) | Melt–$H_2O$–$CO_2$ fluid solubility model http://volcanoes.usgs.gov/observatories/yvo/jlowenstern/other/software_jbl.html |
| Papale et al. (2006) | Melt–$H_2O$–$CO_2$ fluid solubility model http://ctserver.ofm-research.org/Papale/Papale.php |
| Moore (2008) | $H_2O$, $CO_2$, and mixed fluid volatile solubility in magmas Review and critical summary; his Table 3—General models for mixed fluids |
| Wallace and Carmichael (1992), Moretti and Ottonello (2005), Moretti and Baker (2008) | Sulfur solubility and speciation in magmas |
| Kress et al. (2004) | C–O–H–S–Cl–F gas speciation Excel workbook available as journal supplement |
| Connolly (2005) | Phase equilibrium calculations PerpleX: http://serc.carleton.edu/research_education/equilibria/perplex.html |
| Powell et al. (1998) | Phase equilibrium calculations THERMOCALC: http://serc.carleton.edu/research_education/equilibria/thermocalc.html |
| de Capitani and Petrakakis (2010) | Phase equilibrium calculations Theriak/Domino: http://serc.carleton.edu/research_education/equilibria/theriak-domino.html |
| Frank Spear | Phase equilibrium calculations Program Gibbs: http://ees2.geo.rpi.edu/MetaPetaRen/Software/GibbsWeb/Gibbs.html |
| Ariskin (1999) | Phase equilibria in basaltic magmas COMAGMAT: http://geo.web.ru/~kbs/ |
| Ghiorso and Sack (1995), Asimow and Ghiorso (1998), Ghiorso et al. (2002), Gualda et al. (2012) | Magmatic phase equilibria MELTS—low pressure, broad composition range, pMELTS—1–3 GPa, mantle-like bulk compositions, rhyolite-MELTS—like MELTS, with improved modeling of silicic two-feldspar + quartz + fluid-saturated systems http://melts.ofm-research.org/ |
| Asimow et al. (2004), Smith and Asimow (2005), Thompson et al. (2007), Antoshechkina et al. (2010) | Mantle phase equilibria alphaMELTS—pMELTS plus trace elements and water in nominally anhydrous mantle minerals. Numerous option enhancements; batch processing http://magmasource.caltech.edu/alphamelts/ |
| OFM Research | PhasePlot Gridded phase equilibrium calculations for magmatic systems, utilizing the MELTS and pMELTS thermochemical data/model collections http://phaseplot.org/ Macintosh App Store |
| Bohrson and Spera (2001, 2003, 2007), Spera and Bohrson (2001, 2002, 2004), Bohrson et al. (in press) | Energy-constrained open-system magmatic processes http://magma.geol.ucsb.edu/papers/ECAFC.html |
| Kress and Ghiorso (2004) | Postentrapment crystallization of melt inclusions http://brimstone.ess.washington.edu/ |

exchange between coexisting spinel and ilmenite. It should be noted that alternative calibrations of the Fe–Ti oxide geothermometer oxygen barometer exist and can be accessed via QUILF. Finally, the plagioclase hygrometer/thermometer of Lange et al. (2009) is an extraordinarily useful tool for understanding the mutual effect of temperature and melt water content on the stability relations of plagioclase in intermediate to silicic magmas.

Author's personal copy



## 4.2. Mineral and Melt Thermodynamic Property Calculators for Magmatic Phases

Table 6.2 lists several sources of information (all online) for thermodynamic property calculators (pure end-member properties and mixing properties, e.g., activities). When using any of these tools it is very important to understand that pure end-member properties and solution or mineral activities are related through the definition of the chemical potential, as

$$\mu_i = \mu_i^0 + RT \ln a_i \tag{6.4}$$

The only bit of reality in Eqn (6.4) is the end-member chemical potential, $\mu_i$. That quantity and its temperature and pressure derivatives are calibrated against experimental measurement. The chemical potential is partitioned by convenience into a pure end-member contribution ($\mu_i^0$) and an end-member activity ($a_i$), and unless there is independent experimental evidence to fix one or the other, the two are correlated quantities and the model that derives one of these quantities must be internally consistent with the calibration of the other. So, the reader is advised to be very careful in mixing and matching mineral/melt activities with arbitrary pure end-member properties. The two are not always consistent unless care is taken to make them so. Failure to heed this warning can lead to incorrect estimates of solution properties and perhaps erroneous predictions of phase stability, elemental partition, temperature, or pressure.

## 4.3. Solubility Calculators for Volatiles in Magmatic Systems

There are a number of thermodynamically based methods for estimating volatile solubilities in magmatic systems. The majority of work has focused on pure $H_2O$ or pure $CO_2$ fluids; Moore (2008) provides a comprehensive review. For mixed-fluid ($H_2O$–$CO_2$) saturation applications a number of compositionally restricted formulations exist (e.g., Iacono-Marziano et al., 2012), but two general methods are in common use and are listed in Table 6.2. The calibration of Papale et al. (2006) covers the broadest compositional range, and is most generally applied to the interpretation of melt inclusions. Moore (2008) assesses the accuracy of this calibration against experimental measurements.

Almost all the models of $H_2O$ solubility in magmatic liquids make the assumption that the solubility of silicate material in the fluid phase is either negligible or has little effect on the chemical potential of $H_2O$ in the fluid. This assumption is thermodynamically inconsistent, but experimental data are limited to assess the consequences quantitatively. The main exceptions are the $SiO_2$–$H_2O$ and $NaAlSi_3O_8$–$H_2O$ systems, for which experimental data are available to define the extent of solution on both sides of the binary. Hunt and Manning (2012) have calibrated an elegant thermodynamic model for the $SiO_2$–$H_2O$ binary that accounts for the mutual solubility of end-members and the closure of the miscibility gap to form a continuous solution above the second critical endpoint of the system. As interest focuses on the nature of volatile saturation at mantle temperatures and pressures, it will become necessary to extend all of the melt–volatile thermodynamic solubility treatments to incorporate the concept of mutual solubility and complete solution. This is an exciting challenge for the future.

Thermodynamic models describing the solubility of reduced and oxidized sulfur gas species in silicate melts are also listed in Table 6.2. These formulations have yet to be integrated with ferric–ferrous redox calibrations (Kress and Carmichael, 1991) for the melt phase. Coupling the two models and merging the sulfur saturation state models with those for water and carbon dioxide remains another challenge for future thermodynamic models of volatile saturation.

We are not aware of any thermodynamic models of volatile saturation for other components such as Cl, F, or, for that matter, reduced carbon species. If the focus is on the gas state, however, the 2004 model of Kress et al. (2004) may be utilized to estimate species abundances, activities, and fugacities in the system C–O–H–S–Cl–F, on the assumption of ideal mixing.

## 4.4. Computation of Phase Equilibria

We list at the bottom of Table 6.2, descriptions and links to software that perform calculations of phase equilibria (generalized phase diagrams) for both subsolidus crustal- and mantle-like bulk compositions, and for magmatic systems. The latter category includes COMAGMAT, which is optimized for low-pressure, basaltic magmas; MELTS (and rhyolite-MELTS), which is applicable over a broader compositional range, but still restricted to pressures below about 1 GPa; and pMELTS, which is a calibration optimized for mantle-like bulk compositions in the range 1–3 GPa. MELTS and pMELTS consist of collections of thermodynamic models for silicate liquid, mineral, and fluid phases, with the liquid-phase properties derived in part from experimental liquid–solid phase equilibrium data. These models suffer from the serious limitations of incomplete data coverage, inconsistent data, and inadequacies of the underlying thermodynamic solution theory. One particular hindrance is a lack of high-quality experimental data characterizing elemental partitioning between amphibole and liquid and between biotite and liquid. This data deficiency precludes the development of appropriate solution models for these solid phases and

Author's personal copy



prevents modeling magmatic evolution scenarios where either phase plays a dominant role. PhasePlot is an implementation of the MELTS and pMELTS computational infrastructure with a user interface best suited for visualization of phase relations on grids, and for the computation of phase diagrams.

A derivative of the pMELTS thermochemical data/model collection is alphaMELTS (previously phMELTS and Adiabat_1ph) with addition of trace element partitioning and $H_2O$ partitioning into nominally anhydrous phases. It is optimized for a number of computing platforms and can function without a graphical user interface. It is the tool of choice for modeling melt production in the mantle by fractional or batch melting along adiabatic ascent paths.

While MELTS and pMELTS can be utilized to perform modeling in closed or open (to oxygen) systems in either equilibrium crystallization or fractionation modes, they can also be used for isochoric (constant volume, Helmholtz free energy minimization), **isentropic** (constant entropy, enthalpy minimization), and **isenthalpic** (constant enthalpy, entropy maximization) thermodynamic paths. The last is especially useful for exploring energy-constrained assimilation scenarios at constant pressure (Bowen, 1922; Ghiorso and Kelemen, 1987). The EC-AFC models of Bohrson and Spera (Table 6.2) explore this concept and develop a modeling infrastructure for tracking major- and trace-element evolution in a fractionating magma body subjected to energy-constrained assimilation, magma recharge, and periodic eruption. The latest incarnation of this modeling software is termed the Magma Chamber Simulator (Bohrson et al., 2014) that utilizes rhyolite-MELTS as the computational phase equilibrium engine.

The final entry in Table 6.2 is a modeling package aimed at simulating (and reverse calculating) the effects of postentrapment crystallization within melt inclusions trapped within host crystals. The scheme accounts for volume change on crystallization and the constraints imposed upon the inclusion by the thermal expansion and compressibility of the enclosing crystal. The phase equilibrium engine utilized for these calculations is MELTS.

## 5. FUTURE DIRECTIONS OF CHEMICAL THERMODYNAMIC APPLICATIONS IN MAGMATIC SYSTEMS

The application of chemical thermodynamics to the study of magmas has come a long way since the pioneering work of Verhoogen (1949) and Carmichael et al. (1970). These prescient applications of chemical thermodynamics to the study of the origin and evolution of magmas laid the foundation for all subsequent work. Although much has been accomplished over the last half century, much still needs to be done. The future is bright for applications of chemical thermodynamics to magmatic systems. One could say that the whole field is just beginning to mature to facilitate the creation of a working infrastructure for general applications.

One of the main research objectives driving the field is the integration of thermodynamics-based phase property engines into computational fluid dynamics (CFD) simulation of magma chamber processes and melt generation. Until very recently, the computer cycles required to compute phase properties and proportions at each grid node in a CFD computation rendered this level of integration impractical. With the advent of cheap, cluster-based computing and the improvement in numerical algorithms for nonlinear multidimensional optimization, this obstacle is rapidly disappearing. Couple this evolution with the realization that thermodynamic calculations are intrinsically local and can be largely decoupled from neighboring computations in a spatial grid, and it becomes clear that the rate-limiting step in CFD simulations is no longer the time consumed in evaluating the constitutive relations. Casting the CFD simulation in terms of a heat content field rather than a temperature field (e.g., Figure 6.5) serves to nearly eliminate Stefan boundary issues that would otherwise require high-density grid spacing around phase transformation fronts.

Refinement and broadening of chemical thermodynamic models for magmatic systems awaits acquisition of more and better data on the physical properties of earth materials as well as the chemical partitioning of elements between magmatic phases. These data can be acquired by either physical or computational experiment, the latter arising from first-principles and molecular dynamics simulations. Increasingly, the accuracy of first-principles-potential and empirical-potential molecular dynamics simulations of high-temperature silicate liquids and minerals has shown that these tools are capable of generating fundamental data for the purpose of calibration of thermodynamic models (Karki, 2010; Ghiorso and Spera, 2010; Stixrude and Lithgow-Bertelloni, 2010), especially at elevated pressures where traditional physical experimentation is not yet achievable, too costly, or too difficult for routine systematic studies. But, the emergence and success of theoretical computation methods does not diminish the need for high-quality physical experiments. What is desperately needed in this regard are experimental studies aimed specifically at generating data for the calibration of thermodynamic models. This objective requires fully characterized samples through careful chemical analysis and textural documentation, and studies that focus on illuminating the relations between the concentration of an element in a phase and its

Author's personal copy



effective energetic concentration, that is, its activity. That perspective is seldom pursued in phase equilibrium experimentation, but when it is, the results can be spectacular and rewarding beyond the mere documentation of phase relations. Additionally, experimental data that illuminate the fundamental properties (entropy, enthalpy of formation, heat of solution, heat capacity, and equation of state) are by no means complete for magmatic phases, even under crustal conditions. Many of the fundamental data that are used in models that calculate temperatures, pressures, volatile solubilities, or phase relations in magmatic systems are based, in part, on assumed values of thermodynamic constants and internally consistent interpolations or extrapolations of primary data. These models are only as good as their underlying data, and improvement in data quality is both welcome and necessary.

The objective of this chapter on application of chemical thermodynamic to magmatic processes is to highlight the role chemical thermodynamics can play in the day-to-day assessment of petrologic and volcanologic hypotheses. Thermodynamics is the platform upon which kinetic theory is built. It is the framework for our understanding of the systematics of phase equilibria, which provides us with a means of understanding why minerals appear in rocks. It is the underlying theory behind the validity of all geothermometers, geobarometers, and any methods used for the estimation of other intensive variables in magmatic systems. Chemical thermodynamics will continue to play a vital role in making the connection between the chemistry of a magma and its energy, thereby permitting the dynamical evolution of magmatic systems to be coupled directly and quantitatively to the chemical signatures observed in the rock record.

## ACKNOWLEDGMENTS

Material support from the National Science Foundation (EAR 11-19297 to Ghiorso; EAR 1151337 and EAR 0948528 to Gualda) is gratefully acknowledged. The first author is indebted to Jean Verhoogen, Hal Helgeson, and Ian Carmichael, whose astounding contributions to chemical thermodynamics of Earth materials continue to inspire.

## FURTHER READING

Anderson, J.L., Barth, A.P., Wooden, J.L., Mazdab, F., 2008. Thermometers and thermobarometers in granitic systems. In: Putirka, K.D., Tepley III, F.J. (Eds.), Minerals, Inclusions and Volcanic Processes. Reviews in Mineralogy and Geochemistry, vol. 69, pp. 121–142.

Andersen, D.J., Lindsley, D.H., Davidson, P.M., 1993. QUILF: a Pascal program to acces equilibria among Fe-Mg-Ti oxides, pyroxenes, olivine, and quartz. Computers in Geosciences 19, 1333–1350.

Antoshechkina, P.M., Asimow, P.D., Hauri, E.H., Luffi, P.I., 2010. Effect of water on mantle melting and magma differentiation, as modeled using Adiabat_1ph 3.0. In: American Geophysical Union, Fall Meeting 2010 abstract #V53C-2264.

Ariskin, A.A., 1999. Phase equilibria modeling in igneous petrology: use of COMAGMAT model for simulating fractionation of ferro-basaltic magmas and the genesis of high-alumina basalt. Journal of Volcanology and Geothermal Research 90, 115–162.

Asimow, P.D., Dixon, J.E., Langmuir, C.H., 2004. A hydrous melting and fractionation model for mid-ocean ridge basalts: application to the Mid-Atlantic Ridge near the Azores. Geochemistry Geophysics Geosystems 5. http://dx.doi.org/10.1029/2003GC000568.

Asimow, P.D., Ghiorso, M.S., 1998. Algorithmic modifications extending MELTS to calculate subsolidus phase relations. American Mineralogist 83, 1127–1132.

Berman, R.G., 1988. Internally-consistent thermodynamic data for minerals in the system $Na_2O$-$K_2O$-CaO-MgO-FeO-$Fe_2O_3$-$Al_2O_3$-$SiO_2$-$TiO_2$-$H_2O$-$CO_2$. Journal of Petrology 29, 445–522.

Berman, R.G., 2007. winTWQ (version 2.3): a software package for performing internally-consistent thermobarometric calculations. Geological Survey of Canada. Open File 5462, (ed. 2.32), 41 pp.

Bohrson, W.A., Spera, F.J., 2001. Energy-constrained open-system magmatic processes. II: application of energy-constrained assimilation-fractional crystallization (EC-AFC) model to magmatic systems. Journal of Petrology 42, 1019–1041.

Bohrson, W.A., Spera, F.J., 2003. Energy-constrained open-system magmatic processes. IV: geochemical, thermal and mass consequences of energy-constrained recharge, assimilation and fractional crystallization (EC-RAFC). Geochemistry, Geophysics, Geosystems 4. http://dx.doi.org/10.1029/2002GC00316.

Bohrson, W.A., Spera, F.J., 2007. Energy-constrained recharge, assimilation, and fractional crystallization (EC-RA/É'/FC): a Visual Basic computer code for calculating trace element and isotope variations of open-system magmatic systems. Geochemistry, Geophysics, Geosystems 8. http://dx.doi.org/10.1029/2007GC001781.

Bohrson, W.A., Spera, F.J., Ghiorso, M.S., Creamer, J. Thermodynamic model for energy-constrained open system evolution of crustal magma bodies undergoing simultaneous assimilation, recharge and crystallization: the magma chamber simulator. Journal of Petrology, in press.

Bowen, N.L., 1922. The behavior of inclusions in igneous magmas. Journal of Geology 30, 513–570.

Bumstead, H.A., Van Name, R.G. (Eds.), 1906. The Scientific Papers of J. Willard Gibbs. Thermodynamics, vol. 1. Longmans Green and Co., 464 pp.

Callen, H.B., 1985. Thermodynamics and an Introduction to Thermostatics, second ed. John Wiley and Sons, New York. 493 pp.

Carmichael, I.S.E., Ghiorso, M.S., 1990. The effect of oxygen fugacity on the redox state of natural liquids and their crystallizing phases. In: Nicholls, J., Russell, J.K. (Eds.), Modern Methods of Igneous Petrology: Understanding Magmatic Processes. Reviews in Mineralogy and Geochemistry, vol. 24, pp. 191–212.

Carmichael, I.S.E., Nicholls, J., Smith, A.L., 1970. Silica activity in igneous rocks. American Mineralogist 55, 246–263.

Connolly, J.A.D., 2005. Computation of phase equilibria by linear programming: a tool for geodynamic modeling and its application to subduction zone decarbonation. Earth and Planetary Science Letters 236, 524–541.

Author's personal copy



de Capitani, C., Petrakakis, K., 2010. The computation of equilibrium assemblage diagrams with Theriak/Domino software. American Mineralogist 95, 1006–1016.

Ferry, J.M., Watson, E.B., 2007. New thermodynamic models and revised calibrations for the Ti-in-zircon and Zr-in-rutile thermometers. Contributions to Mineralogy and Petrology 154, 429–437.

Fowler, S.J., Spera, F.J., Bohrson, W.A., Belkin, H.E., de Vivo, B., 2007. Phase equilibria constraints on the chemical and physical evolution of the Campanian Ignimbrite. Journal of Petrology 48, 459–493.

Ganguly, J., 2008. Thermodynamics in Earth and Planetary Sciences. Springer-Verlag, Berlin, 501 pp.

Ghiorso, M.S., 1985. Chemical mass transfer in magmatic processes. I. Thermodynamic relations and numerical algorithms. Contributions to Mineralogy and Petrology 90, 107–120.

Ghiorso, M.S., 1997. Thermodynamic models of igneous processes. Annual Reviews of Earth and Planetary Sciences 25, 221–241.

Ghiorso, M.S., 2013. A globally convergent saturation state algorithm applicable to thermodynamic systems with a stable or metastable omnicomponent phase. Geochimica et Cosmochimica Acta 103, 295–300.

Ghiorso, M.S., Carmichael, I.S.E., 1985. Chemical mass transfer in magmatic processes. II. Applications in equilibrium crystallization, fractionation and assimilation. Contributions to Mineralogy and Petrology 90, 121–141.

Ghiorso, M.S., Evans, B.W.E., 2008. Thermodynamics of rhombohedral oxide solid solutions and a revision of the Fe-Ti two-oxide geothermometer and oxygen-barometer. American Journal of Science 308, 957–1039.

Ghiorso, M.S., Gualda, G.A.R., 2012. A method for estimating the activity of titania in magmatic liquids from the compositions of coexisting rhombohedral and cubic iron–titanium oxides. Contributions to Mineralogy and Petrology 165, 73–81.

Ghiorso, M.S., Hirschmann, M.M., Reiners, P.W., Kress III, V.C., 2002. The pMELTS: A revision of MELTS for improved calculation of phase relations and major element partitioning related to partial melting of the mantle to 3 GPa. Geochemistry, Geophysics, Geosystems 3. http://dx.doi.org/10.1029/2001GC000217.

Ghiorso, M.S., Kelemen, P.B., 1987. Evaluating reaction stoichiometry in magmatic systems evolving under generalized thermodynamic constraints: examples comparing isothermal and isenthalpic assimilation. In: Mysen, B. (Ed.), Magmatic Processes: Physiochemical Principles, Geochemical Society Special Publication, vol. 1, pp. 319–336.

Ghiorso, M.S., Kress, V.C., 2004. An equation of state for silicate melts. II. Calibration of volumetric properties at $10^5$ Pa. American Journal of Science 204, 679–751.

Ghiorso, M.S., Sack, R.O., 1995. Chemical mass transfer in magmatic processes. IV. A revised and internally consistent thermodynamic model for the interpolation and extrapolation of solid-liquid equilibria in magmatic systems at elevated temperatures and pressures. Contributions to Mineralogy and Petrology 119, 197–212.

Ghiorso, M.S., Spera, F.J., 2010. Large scale simulations. In: Wentzcovitch, R., Stixrude, L. (Eds.), Theoretical and Computational Methods in Mineral Physics. Reviews in Mineralogy and Geochemistry, vol. 71, pp. 437–462.

Gibbs, J.W., 1878. On the equilibrium of heterogeneous substances. Transactions of the Connecticut Academy III, 108–248 and 343–524.

Gualda, G.A.R., Ghiorso, M.S., Lemons, R.V., Carley, T.L., 2012. Rhyolite-MELTS: a modified calibration of MELTS optimized for silica-rich, fluid-bearing magmatic systems. Journal of Petrology 53, 875–890.

Gualda, G.A.R., Ghiorso, M.S., 2014. Phase-equilibrium geobarometers for silicic rocks based on rhyolite-MELTS. Contributions to Mineralogy and Petrology 168, 1033.

Hayden, L.A., Watson, E.B., Wark, D.A., 2008. A thermobarometer for sphene (titanite). Contributions to Mineralogy and Petrology 155, 529–540.

Huang, R., Audetat, A., 2012. The titanium-in-quartz (TitaniQ) thermobarometer: a critical examination and re-calibration. Geochimica et Cosmochimica Acta 84, 75–89.

Hunt, J.D., Manning, C.E., 2012. A thermodynamic model for the system $SiO_2$–$H_2O$ near the upper critical end point based on quartz solubility experiments at 500–1100 °C and 5–20 kbar. Geochimica et Copsmochimica Acta 86, 196–213.

Iacono-Marziano, G., Morizet, Y., le Trong, E., Gaillard, F., 2012. New experimental data and semi-empirical parameterization of $H_2O$–$CO_2$ solubility in mafic melts. Geochimica et Cosmochimica Acta 97, 1–23.

Karki, B.B., 2010. First-principles molecular dynamics simulations of silicate melts: structural and dynamical properties. In: Wentzcovitch, R., Stixrude, L. (Eds.), Theoretical and Computational Methods in Mineral Physics. Reviews in Mineralogy and Geochemistry, vol. 71, pp. 355–386.

Kress, V.C., 1997. Thermochemistry of sulfide liquids I. The system O-S-Fe at 1 bar. Contributions to Mineralogy and Petrology 127, 176–186.

Kress, V.C., 2000. Thermochemistry of sulfide liquids II. Associated solution model for sulfide liquids in the system O-S-Fe. Contributions to Mineralogy and Petrology 139, 316–325.

Kress, V.C., 2007. Thermochemistry of sulfide liquids III. Ni-bearing liquids at 1-bar. Contributions to Mineralogy and Petrology 154, 191–204.

Kress, V.C., Carmichael, I.S.E., 1991. The compressibility of silicate liquids containing $Fe_2O_3$ and the effect of composition, temperature, oxygen fugacity and pressure on their redox states. Contributions to Mineralogy and Petrology 108, 82–92.

Kress, V.C., Ghiorso, M.S., 2004. Thermodynamic modeling of post-entrapment crystallization in igneous phases. Journal of Volcanology and Geothermal Research 137, 247–260.

Kress, V.C., Ghiorso, M.S., Lastuka, C., 2004. Microsoft EXCEL spreadsheet-based program for calculating equilibrium gas speciation in the C-O-H-S-Cl-F system. Computers and Geosciences 30, 211–214.

Kress, V.C., Greene, L.E., Ortiz, M.D., Mioduszewski, L., 2008. Thermochemistry of sulfide liquids IV: density measurements and the thermodynamics of O–S–Fe–Ni–Cu liquids at low to moderate pressures. Contributions to Mineralogy and Petrology 156, 785–797.

Lange, R.A., Carmichael, I.S.E., 1990. Thermodynamic properties of silicate liquids with emphasis on density, thermal expansion and compressibility. In: Nicholls, J., Russell, J.K. (Eds.), Modern Methods of Igneous Petrology: Understanding Magmatic Processes. Reviews in Mineralogy and Geochemistry, vol. 24, pp. 25–64.

Lange, R.A., Frey, H.M., Hector, J., 2009. A thermodynamic model for the plagioclase-liquid hygrometer/thermometer. American Mineralogist 94, 494–506.

Moore, G., 2008. Interpreting $H_2O$ and $CO_2$ contents in melt inclusions: constraints from solubility experiments and modeling. In:

Author's personal copy



Putirka, K.D., Tepley III, F.J. (Eds.), Minerals, Inclusions and Volcanic Processes. Reviews in Mineralogy and Geochemistry, vol. 69, pp. 333–361.

Moretti, R., Baker, D.R., 2008. Modeling the interplay of $fO_2$ and $fS_2$ along the FeS-silicate melt equilibrium. Chemical Geology 256, 286–298.

Moretti, R., Ottonello, G., 2005. Solubility and speciation of sulfur in silicate melts, the Conjugated Toop–Samis–Flood–Grjotheim (CTSFG) model. Geochimica Cosmochimica Acta 69, 801–823.

Newman, S., Lowenstern, J.B., 2002. VolatileCalc: a silicate melt–$H_2O$–$CO_2$ solution model written in Visual Basic for excel. Computers and Geosciences 28, 597–604.

Osborn, E.F., 1959. Role of oxygen pressure in the crystallization and differentiation of basaltic magma. American Journal of Science 257, 609–647.

Osborn, E.F., 1962. Reaction series for sub-alkaline igneous rocks based on different oxygen pressure conditions. American Mineralogist 47, 211–226.

Papale, P., Moretti, R., Barbato, D., 2006. The compositional dependence of the saturation surface of $H_2O + CO_2$ fluids in silicate melts. Chemical Geology 229, 78–95.

Pitzer, K.S., Brewer, L., 1961. Thermodynamics. McGraw-Hill, New York, 723 pp.

Powell, R., Holland, T.J.B., Worley, B., 1998. Calculating phase diagrams involving solid solutions via non-linear equations, with examples using THERMOCALC. Journal of Metamorphic Geology 16, 577–588.

Prigogine, I., Defay, R., 1954. Chemical Thermodynamics. Longmans Green and Co., London, 543 pp.

Putirka, K.D., 2008. Thermometers and barometers for volcanic systems. In: Putirka, K.D., Tepley III, F.J. (Eds.), Minerals, Inclusions and Volcanic Processes. Reviews in Mineralogy and Geochemistry, vol. 69, pp. 61–120.

Sack, R.O., Ghiorso, M.S., 1991. Chromium spinels as petrogenetic indicators: thermodynamics and petrological applications. American Mineralogist 87, 79–98.

Smith, P.M., Asimow, P.D., 2005. Adiabat_1ph: a new public front-end to the MELTS, pMELTS, and pHMELTS models. Geochemistry, Geophysics, Geosystems 6. http://dx.doi.org/10.1029/2004GC000816.

Spear, F.S., 1993. Metamorphic Phase Equilibria and Pressure-Temperature-Time Paths. Mineralogical Society of America Monograph, 799 pp.

Spera, F.J., Bohrson, W.A., 2001. Energy-constrained open-system magmatic processes. I: general model and energy-constrained assimilation and fractional crystallization (EC-AFC) formulation. Journal of Petrology 42, 999–1018.

Spera, F.J., Bohrson, W.A., 2002. Energy-constrained open-system magmatic processes. III: energy-constrained recharge, assimilation and fractional crystallization (EC-RAFC). Geochemistry, Geophysics, Geosystems 3. http://dx.doi.org/10.1029/2002GC00315.

Spera, F.J., Bohrson, W.A., 2004. Open-system magma chamber evolution: an energy-constrained geochemical model incorporating the effects of concurrent eruption, recharge, variable assimilation and fractional crystallization (EC-E'RAFC). Journal of Petrology 45, 2459–2480.

Stixrude, L., Lithgow-Bertelloni, C., 2010. Thermodynamics of the Earth's mantle. In: Wentzcovitch, R., Stixrude, L. (Eds.), Theoretical and Computational Methods in Mineral Physics. Reviews in Mineralogy and Geochemistry, vol. 71, pp. 465–484.

Thomas, J.B., Watson, E.B., Spear, F.S., 2010. TitaniQ under pressure: the effect of pressure and temperature on the solubility of Ti in quartz. Contributions to Mineralogy and Petrology 160, 743–759.

Thompson, R.N., Riches, A.J.V., Antoshechkina, P.M., Pearson, D.G., Nowell, G.M., Ottley, C.J., Dickin, A.P., Hards, V.L., Nguno, A.-K., Niku-Paavola, V., 2007. Origin of CFB magmatism: multi-tiered intracrustal picrite–rhyolite magmatic plumbing at Spitzkoppe, Western Namibia, during Early Cretaceous Etendeka magmatism. Journal of Petrology 48, 1119–1154.

Verhoogen, J., 1949. Thermodynamics of a magmatic gas phase, vol. 28. University of California Publications. Bulletin of the Department of Geological Sciences, 91–135.

Wallace, P., Carmichael, I.S.E., 1992. Sulfur in basaltic magma. Geochimica et Cosmochimica Acta 56, 1863–1874.

Wark, D.A., Watson, E.B., 2006. TitaniQ: a titanium-in-quartz geothermometer. Contributions to Mineralogy and Petrology 152, 743–754.

Watson, E.B., Wark, D.A., Thomas, J.B., 2006. Crystallization thermometers for zircon and rutile. Contributions to Mineralogy and Petrology 151, 413–433.